Fluctuation loops in noise-driven linear dynamical systems

Akhil Ghanta,[1] John C. Neu,[2] and Stephen Teitsworth[1,*]
[1]*Duke University, Department of Physics, Box 90305 Durham, North Carolina 27708-0305, USA*
[2]*Duke University, Department of Biomedical Engineering, Box 90281 Durham, North Carolina 27708-0281, USA*
(Received 30 December 2016; published 16 March 2017)

Understanding the spatiotemporal structure of most probable fluctuation pathways to rarely occurring states is a central problem in the study of noise-driven, nonequilibrium dynamical systems. When the underlying system does not possess detailed balance, the optimal fluctuation pathway to a particular state and relaxation pathway from that state may combine to form a looplike structure in the system phase space called a *fluctuation loop*. Here, fluctuation loops are studied in a linear circuit model consisting of coupled RC elements, where each element is driven by its own independent noise source. Using a stochastic Hamiltonian approach, we determine the optimal fluctuation pathways, and analytically construct corresponding fluctuation loops. To quantitatively characterize fluctuation loops, we study the time-dependent area tensor that is swept out by individual stochastic trajectories in the system phase space. At long times, the area tensor scales linearly with time, with a coefficient that precisely vanishes when the system satisfies detailed balance.

DOI: 10.1103/PhysRevE.95.032128

I. INTRODUCTION

Noise-induced transitions to rarely occurring states play an important role in processes throughout the natural sciences such as neuron dynamics [1], climate modeling [2–5], nonlinear electronic transport structures [6], and micromechanical oscillators [7,8]. Two central questions associated with such transitions are (1) how do they occur dynamically, i.e., what is the typical time that it takes to reach a rare state from a given initial state, and (2) what is the most likely path through phase space to reach the rare state? An important subclass of systems exhibiting this type of behavior can be represented as a high-dimensional and *linear* set of stochastic differential equations. Such models typically arise through the linearization of nonlinear and nonequilibrium models about stable fixed points. In addition, there are important physical systems that are well described as linear stochastic dynamical systems, for example, climate models for predicting El Niño events [2] and models for active biological systems such as beating flagella [9] and fluctuations in the actin cytoskeleton of cells [10]. Interestingly, such systems, including the preceding two examples, typically do not possess *detailed balance* when they describe systems that are not in thermal equilibrium. Most previous work on such systems has focused on numerical simulation of systems of linear Langevin equations [2,11,12], with relatively little analytical work concerning the dynamics of optimal fluctuational paths. In this paper, we focus on the analytical derivation and numerical exposition of fluctuation loops which generically occur in systems that do not possess detailed balance.

We start by considering a stochastic dynamical system that is characterized by a deterministic velocity field on N-dimensional configuration space, and a state-independent noise tensor. We assume that the velocity field has critical points, and we take the origin $\mathbf{x} = 0$ of configuration space to coincide with one of them. We examine stochastic trajectories in a sufficiently small neighborhood of $\mathbf{x} = 0$, where the velocity field $\mathbf{u}(\mathbf{x})$ is well approximated by its linearization,

$$\mathbf{u}(\mathbf{x}) \sim J\mathbf{x}, \tag{1}$$

where J is the Jacobian tensor at $\mathbf{x} = 0$. Within this linear approximation, the stochastic differential equation (SDE) that produces stochastic trajectories $\mathbf{x} = \mathbf{x}(t)$ can be written:

$$\dot{\mathbf{x}} = J\mathbf{x} + \sigma\mathbf{w}(t), \tag{2}$$

where each component of $\mathbf{w}(t)$ is an independent unit white noise, and σ is the state-independent noise tensor. Each component $w_i(t)$ of $\mathbf{w}(t)$ is a *unit* white noise if the associated Brownian motion $B_i(t) := \int_0^t w_i(t')dt'$ has mean square deviation $\langle B_i^2(t)\rangle = 2t$.

Detailed balance, or breaking thereof, refers to a property of the stochastic differential equation (2). Letting $\rho(\mathbf{x},t)$ denote the ensemble probability density, the associated probability current is

$$\mathbf{j}(\mathbf{x},\mathbf{t}) = J\mathbf{x}\rho(\mathbf{x},t) - D\nabla\rho(\mathbf{x},t), \tag{3}$$

where $D := \sigma\sigma^T$ denotes the diffusion tensor. Suppose we isolate a bounded region of configuration space with nonabsorbing walls (i.e., vanishing normal component of $\mathbf{j}$ on the boundary) and the density inside relaxes to a time independent steady state. Then, we have detailed balance if the steady $\mathbf{j}$ vanishes identically throughout the interior, and

$$\nabla \log \rho = \frac{\nabla\rho}{\rho} = D^{-1}J\mathbf{x}. \tag{4}$$

The right hand side of (4) is a gradient only if $D^{-1}J$ is symmetric. Equivalently, the *stochastic vorticity tensor* ω with components

$$\omega_{ij} = (D^{-1}J)_{ji} - (D^{-1}J)_{ij} \tag{5}$$

vanishes identically [13]. Breaking of detailed balance means that there is no density that gives $\mathbf{j} = 0$, because the vorticity is nonzero.

Detailed balance or its breaking is manifested in the individual stochastic trajectories. If $\mathbf{x} = 0$ is a stable critical point, stochastic trajectories spend most of their time within a characteristic distance of the origin $l \sim |D^{-1}J|$ [14]. Rarely, a stochastic trajectory will reach some small neighborhood of a distant destination point $\mathbf{x} = \mathbf{b}$, far from $\mathbf{x} = 0$ in the sense $|\mathbf{b}| \gg l$. Subsequently, it will typically relax quickly

*teitso@phy.duke.edu

back to within $O(l)$ of $\mathbf{x} = 0$. Such stochastic trajectories in configuration space are called *fluctuation loops*. Provided that the noise intensity is sufficiently small, large deviation theory [15,16] predicts that the segment of loop from zero to $\mathbf{b}$ closely follows a unique most probable escape path, and the segment from $\mathbf{b}$ to zero closely follows the deterministic relaxation path from $\mathbf{b}$ to zero. In a detailed balance system, the escape segment is the reversal in both space and time of the relaxation segment [12]. If detailed balance is broken, the escape and relaxation segments do not coincide.

The structure of the paper is as follows. Section II presents the construction of fluctuation loops for the linearized stochastic dynamics by solving the effective Hamilton equations of motion of large deviation theory [12,15,17]. Section III applies this construction to a simple network of two coupled RC circuits which is also a good candidate for actual physical experiments. More generally, such linear coupled circuit models are often useful for describing the dynamics of nonlinear electronic transport systems (e.g., semiconductor superlattices and tunnel diodes) in the neighborhood of their stable equilibria [6,18]. The state space is two dimensional, so the fluctuation loops are plane curves. Section IV presents a dynamical area tensor, the time evolution of which provides a quantitative characterization of detailed balance breaking. Given the segment C of a stochastic trajectory in configuration space corresponding to times between zero and t, the area tensor $A(t)$ is defined by its components:

$$A_{ij}(t) := \int_C x_i dx_j - x_j dx_i. \tag{6}$$

Furthermore, we show that the ensemble average $\langle A \rangle$ is zero for a detailed balance system. However, if detailed balance is broken, its time rate of change $d\langle A \rangle/dt$ is found to asymptote to a nonzero constant which is equivalent to the long time limit of the *single* trial ratio $A(T)/T$ as $T \to \infty$. The paper concludes with two Appendices, the first of which derives a pair of fluctuation-dissipation theorems that are useful for nondetailed balance systems. The second Appendix explores the connection between detailed balance breaking and nonequilibrium thermodynamics for the RC network of Sec. III.

II. BASIC THEORY OF FLUCTUATION LOOPS IN LINEAR STOCHASTIC DYNAMICAL SYSTEMS

The construction of fluctuation loops is based on the Hamiltonian dynamics of most probable paths in the small noise limit, with effective Hamiltonian [15,17,19]:

$$H = \mathbf{p} \cdot (D\mathbf{p} + J\mathbf{x}). \tag{7}$$

Here, $\mathbf{x}$ in $\mathbb{R}^N$ is the vector of configuration space coordinates, and $\mathbf{p}$ is the vector of conjugate momenta. We assume that the Jacobian tensor has a complete set of eigenvectors, and that the diffusion tensor D is symmetric and nonsingular. The Hamilton equations are

$$\dot{\mathbf{p}} = -J^T \mathbf{p}, \tag{8}$$

$$\dot{\mathbf{x}} - J\mathbf{x} = 2D\mathbf{p}. \tag{9}$$

The linear momentum dynamics (8) is decoupled from $\mathbf{x}$, and this suggests that the $2N$-dimensional vector space of solutions to (8),(9) be represented as the direct sum of deterministic and momentum subspaces. The N-dimensional deterministic subspace is characterized by $\mathbf{p}(t) = 0$, and $\mathbf{x}(t)$ is a deterministic trajectory in configuration space satisfying $\dot{\mathbf{x}} = J\mathbf{x}$. If the eigenvalues of J all have negative real parts, then $\mathbf{x} = 0$ is a stable critical point, and deterministic trajectories $\mathbf{x}(t)$ decay exponentially to zero. This means that the relaxation segments of fluctuation loops lie in the deterministic subspace. The N-dimensional momentum subspace consists of curves $(\mathbf{x}(t), \mathbf{p}(t))$ in $\mathbb{R}^{2N}$, where $\mathbf{p}(t)$ is a solution of the momentum dynamics (8), and $\mathbf{x}(t)$ is a solution of (9), uniquely determined by $\mathbf{p}(t)$. When $\mathbf{x} = 0$ is a stable critical point, this unique determination is simple: the eigenvalues of $-J^T$ are negatives of the eigenvalues of J, so all nonzero momentum trajectories $\mathbf{p}(t)$ are exponentially growing in t. Given any one of these, the corresponding $\mathbf{x}(t)$ is the unique solution of (9) which vanishes as $t \to -\infty$. Thus the escape segment of fluctuation loops lie in the momentum subspace.

For $(\mathbf{x}, \mathbf{p})$ in the momentum subspace, the unique $\mathbf{x}(t)$ associated with $\mathbf{p}(t)$ is determined by a mapping tensor M such that

$$\mathbf{x}(t) = M\mathbf{p}(t). \tag{10}$$

Substituting (10) for $\mathbf{x}(t)$ into (9) and using (8), we find

$$JM\mathbf{p} + MJ^T\mathbf{p} = -2D\mathbf{p}. \tag{11}$$

Equation (11) holds for all $\mathbf{p}$ in $\mathbb{R}^N$ provided that

$$JM + MJ^T = -2D, \tag{12}$$

a matrix Lyapunov equation which can be shown to have a unique, nonsingular solution for M provided that D is nonsingular [20]. For the case of a stable fixed point where all of the eigenvalues of J have negative real part, the solution can be explicitly written in the form [21]

$$M = 2\int_0^\infty d\tau\, e^{J\tau} D\, e^{J^T\tau}. \tag{13}$$

We are now in a position to assert the following properties for fluctuation loops about a stable critical point. If the eigenvalues of J all have negative real part and the diffusion tensor D is positive, then (12) has a unique symmetric, nonsingular solution for M. Given the N-dimensional vector space of exponentially growing momentum trajectories $\mathbf{p}(t)$, we have an N-dimensional vector space of escape trajectories $\mathbf{x}(t)$ in configuration space induced by the mapping (10). Hence we can reach any destination point $\mathbf{b}$ in configuration space by an escape trajectory from the origin. Finally, the relaxation segment of the fluctuation loop is determined by the solution of the deterministic equation, $\dot{\mathbf{x}} = J\mathbf{x}$, starting from $\mathbf{b}$.

III. CAPACITIVELY COUPLED RC CIRCUIT MODEL AND ITS NONDIMENSIONALIZATION

To make the construction of fluctuations loops concrete, we analyze a two-dimensional, capacitively coupled network of RC circuit elements, where each element is driven by an independent noise source. In the circuit of Fig. 1, $v_1(t)$ and $v_2(t)$ denote voltages at the upper left and right nodes, respectively. The lower two nodes are grounded, with voltage set to zero.

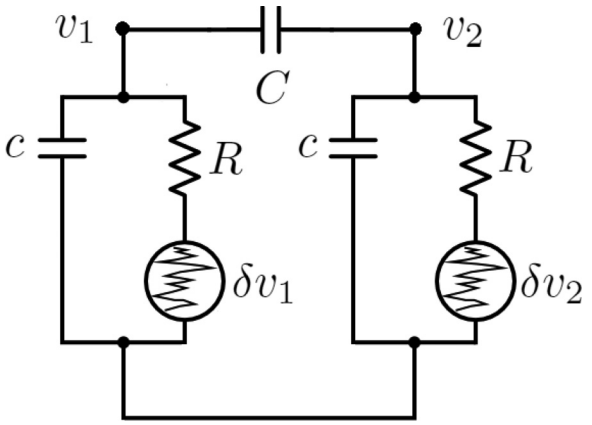

FIG. 1. Two-element, capacitively coupled network of RC circuit elements, each with its own independent noise source.

We have included noise sources in series with the resistors R. The noise voltages are

$$\delta v_i = s_j w_j(t), \quad j = 1,2, \tag{14}$$

where $w_1(t)$ and $w_2(t)$ are independent unit white noises and s_1 and s_2 are given noise amplitudes [22]. Detailed balance is broken by taking the noise amplitudes to be different from one another. In the system, the presence of a large deviation corresponds physically to the development of a large "spontaneous" voltage across one or both of the resistors, after which the system quickly relaxes back to the neighborhood of the zero voltage state.

The circuit dynamical equations for $v_1(t)$ and $v_2(t)$ are

$$c\dot{v}_1 - C(\dot{v}_2 - \dot{v}_1) = -\frac{v_1 - s_1 w_1(t)}{R}, \tag{15a}$$

$$c\dot{v}_2 - C(\dot{v}_1 - \dot{v}_2) = -\frac{v_2 - s_2 w_2(t)}{R}. \tag{15b}$$

Introducing the half-difference and average of voltages,

$$x_1 := \frac{v_2 - v_1}{2}, \quad x_2 := \frac{v_1 + v_2}{2}, \tag{16}$$

and transforming to dimensionless time in units Rc, the equivalent dynamical system for $x_1(t)$, $x_2(t)$ is

$$\dot{x}_1 = -\mu x_1 - \frac{\mu s_1}{2} w_1 + \frac{\mu s_2}{2} w_2, \tag{17a}$$

$$\dot{x}_2 = -x_2 + \frac{s_1}{2} w_1 + \frac{s_2}{2} w_2, \tag{17b}$$

where μ is the dimensionless parameter

$$\mu := \frac{1}{1 + \frac{2C}{c}}. \tag{18}$$

The Jacobian, noise, and diffusion tensors of this stochastic dynamical system are respectively given by

$$J = \begin{pmatrix} -\mu & 0 \\ 0 & -1 \end{pmatrix}, \tag{19}$$

$$\sigma = \frac{1}{2}\begin{pmatrix} -\mu s_1 & \mu s_2 \\ s_1 & s_2 \end{pmatrix}, \tag{20}$$

$$D = \sigma\sigma^T = \begin{pmatrix} \mu^2(d_1 + d_2) & \mu(d_2 - d_1) \\ \mu(d_2 - d_1) & d_1 + d_2 \end{pmatrix}, \tag{21}$$

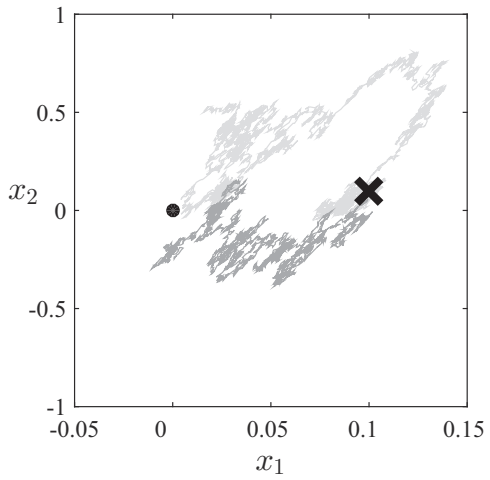

FIG. 2. Numerically generated segment of stochastic trajectory passing through the target region (marked by a cross) and showing a clockwise looping structure. Noise intensities are $d_1 = 0.01$ and $d_2 = 0.1$ so that the system violates detailed balance.

where

$$d_i := \frac{{s_i}^2}{4}, \quad i = 1,2. \tag{22}$$

The vorticity is

$$\omega := (D^{-1}J)_{21} - (D^{-1}J)_{12} = \frac{1}{4}\left(\frac{1}{\mu} - 1\right)\left(\frac{1}{d_2} - \frac{1}{d_1}\right), \tag{23}$$

or, using the definition of μ from (18),

$$\omega = \frac{C}{2c}\left(\frac{1}{d_2} - \frac{1}{d_1}\right). \tag{24}$$

We observe that the sense of circulation is determined by the sign of the (scalar) vorticity ω: clockwise for $\omega < 0$, counterclockwise for $\omega > 0$.

The velocity field $\mathbf{u} = J\mathbf{x}$ with J in (19) represents independent relaxations of x_1, x_2 to zero with dimensionless time constants μ and 1, respectively. Physically, x_1 is proportional to the charge on the "connecting" capacitor C, so the x_1 relaxation expresses the discharging of this connecting capacitor. If $x_1 = 0$, only the capacitors c in parallel with resistors R have nonzero charge, and the relaxation of x_2 represents the discharge of these capacitors. In the limit $0 < \mu \ll 1$, the x_2 relaxation is much faster than the x_1 relaxation, and the critical point $(x_1,x_2) = (0,0)$ is a fast slow node.

Figure 2 shows direct numerical simulation of the circuit SDE (using Euler-Maruyama integration) for parameter values $\mu = 0.1$ and $d_2 = 10d_1 = 0.1$, i.e., the difference in noise intensities is relatively large. The fluctuational part of the trajectory is shown in gray and is constructed by plotting the system position for several dimensionless time units prior to its first hitting a small target ball marked by a cross. The relaxational part of the trajectory is shown in black and is obtained by plotting the system position for the next several dimensionless time units as the system relaxes towards the stable equilibrium. The looping structure and clockwise circulation are clearly apparent; furthermore, different individual trials reveal qualitatively similar behavior. On the

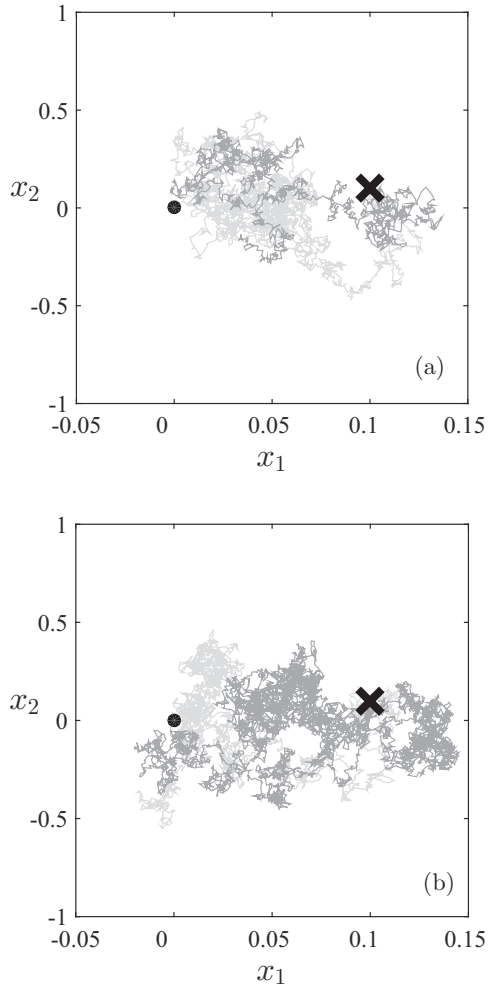

FIG. 3. (a) Numerically generated segment of stochastic trajectory passing through the target region under detailed balance conditions with noise intensities are $d_1 = d_2 = 0.1$. (b) Segment of stochastic trajectory computed for parameters $d_1 = 0.1$ and $d_2 = 0.09$. The system is nondetailed balance but the expected looping structure is *not* discernible.

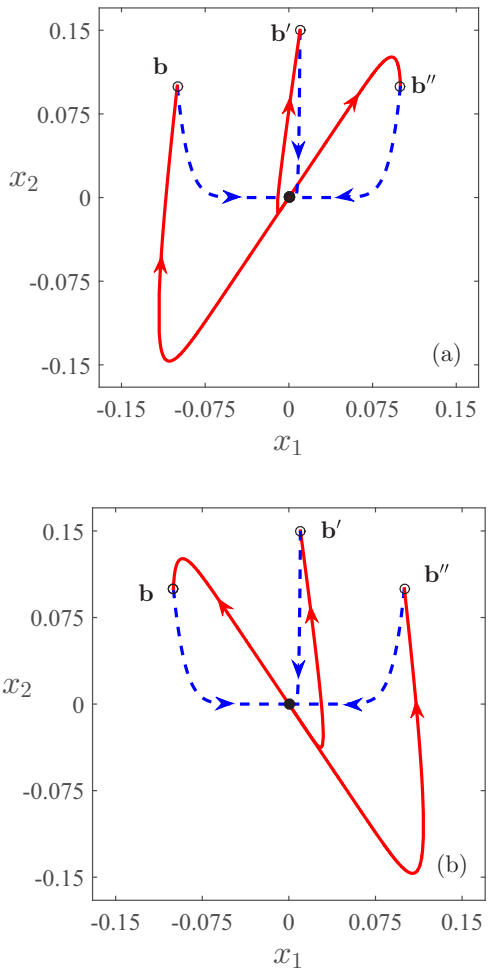

FIG. 4. (a) Calculated most-probable fluctuational and relaxational paths for clockwise vorticity: $d_1 = 0.01$, $d_2 = 0.1$, and $\mu = 0.1$. (b) Calculated most-probable fluctuational and relaxational paths for counterclockwise vorticity: $d_1 = 0.1$, $d_2 = 0.01$, and $\mu = 0.1$.

other hand, when the difference in noise intensities is smaller, it becomes increasingly difficult to distinguish between the detailed balance and nondetailed balance behavior by simply plotting the time-dependent system position. Thus Fig. 3(a) shows typical fluctuational and relaxational trajectories for detailed balance conditions corresponding to parameters $d_2 = d_1 = 0.1$: as expected, there is no apparent vorticity. However, Fig. 3(b) shows the trajectories for parameters $d_1 = 0.1$ and $d_2 = 0.09$, which violates detailed balance. In this case, while the theory indicates a nonzero vorticity [cf. Eq. (5)], it is not possible to discern characteristic looping behavior by simply plotting the individual stochastic trajectories.

We turn now to the analytical construction of the most-probable escape path: given J and D in (19), (21), the solution of (12) for the mapping tensor is

$$M = \begin{pmatrix} \mu(d_1+d_2) & \frac{2\mu}{1+\mu}(d_2-d_1) \\ \frac{2\mu}{1+\mu}(d_2-d_1) & d_1+d_2 \end{pmatrix}. \tag{25}$$

Given an eigenvalue λ of J, and a corresponding left eigenvector $\mathbf{p}$, any multiple of

$$\mathbf{x}(t) := e^{\lambda t} M\mathbf{p} \tag{26}$$

is an escape trajectory. The eigenvalues of J are $-\mu$ and -1 with respective left eigenvectors:

$$(1 \quad 0), \quad (0 \quad 1). \tag{27}$$

Using (26), the specific trajectories are

$$e^{\mu t}\begin{pmatrix} 1+\mu \\ \frac{2(d_2-d_1)}{d_1+d_2} \end{pmatrix}, \quad e^{t}\begin{pmatrix} \mu\frac{2(d_2-d_1)}{d_1+d_2} \\ 1+\mu \end{pmatrix}, \tag{28}$$

and the general escape trajectory is a linear combination of these. The vector coefficients of the exponentials in (28) represent "slow" and "fast" escape directions. Figures 4(a) and 4(b) show the calculated fluctuation loops for three typical "destination" points, $\mathbf{b}$, $\mathbf{b}'$, and $\mathbf{b}''$.

Escape segments of fluctuation loops connecting the origin $(x_1,x_2) = (0,0)$ to these destination points are solid red lines, and the relaxation segments are dashed blue lines. The orientations of fluctuation loops are indicated by the sign of the vorticity (23). The clockwise loops in Fig. 4(a) are based on

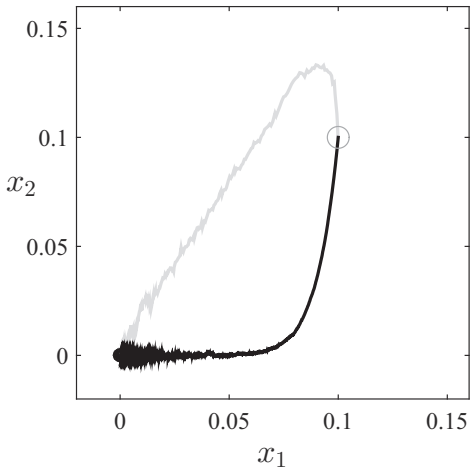

FIG. 5. Most probable escape path (MPEP) and relaxation path (RP) determined by averaging 744 individual trajectories using a target ball centered at (0.1,0.1). System parameters are $\mu = 0.1$, $\epsilon = 0.01$, $d_1 = 0.01$, and $d_2 = 0.1$.

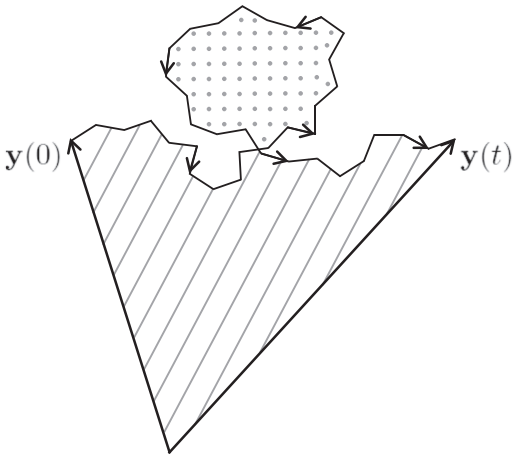

FIG. 6. Area swept by a diffusing particle. The striped region represents positive area, while the dotted region is negative area. The total area swept is the area of the striped region minus the area of the dotted region.

$d_2 = 0.1 > 0.01 = d_1$, for which the vorticity (23) is negative. The shape of the calculated fluctuational trajectories can be qualitatively understood by recalling that d_2 is proportional to the noise intensity associated with the dynamical variable $v_2 := x_1 + x_2$. Thus, for $d_2 \gg d_1$, noisy fluctuations will tend to align with the direction associated with v_2, i.e., $x_2 \simeq x_1$. More precisely, for $\mu \ll 1$, fluctuational trajectories near the origin will tend to lie parallel to the line $x_2 = \frac{2(d_2-d_1)}{(d_1+d_2)(1+\mu)}x_1$, associated with the slow escape direction of (28). Referring to Fig. 4(a), this implies a relatively short fluctuational path to target point $\mathbf{b}''$, which moves out from the origin along the line $x_2 \simeq 1.49x_1$. On the other hand, the fluctuational path to $\mathbf{b}$ is much longer since it first moves out from the origin along $x_2 \simeq 1.49x_1$ into the lower left-hand quadrant before swinging up to $\mathbf{b}$ along the fast direction of (28), i.e., in a direction parallel to the line $x_2 \simeq 6.72x_1$. In Fig. 4(b) with values of d_1, d_2 reversed, the orientation of loops is counterclockwise, and the sign of the vorticity changes to positive. In this case, we can see that the fluctuational paths move away from the origin along the slow direction calculated for these d_i values using (28), i.e., parallel to the line $x_2 \simeq -1.49x_1$.

Figure 5 depicts conditioned, ensemble-averaged $x_1 - x_2$ phase plane trajectories based on direct numerical solutions of the stochastic ODE (17). Trajectories are launched at $t = 0$ from an initial disk about the origin with radius $l \sim |D^{-1}J|$. During a maximum specified run time, a small subset of these trajectories reach a destination disk of radius l about point $\mathbf{b}$, $|\mathbf{b}| \gg l$. Given any one of these, we record the time of flight T_1 from the initial disk to the destination disk, and then continue the trajectory from $t = T_1$ until it again reaches the initial disk at time $t = T_1 + T_2$. The phase plane trajectory depicted in Fig. 5 is the result of averaging 744 individual trials over the time interval $0 < t < \langle T_1 + T_2 \rangle$.

IV. STOCHASTIC AREA TENSOR: QUANTIFYING THE FLUCTUATION LOOPS

We now present a quantitative diagnostic, based on the recorded history of a single stochastic trajectory $\mathbf{x}(t)$, that allows us to detect the breaking of detailed balance in the underlying dynamics. This diagnostic does not require knowledge of the Jacobian J, nor of the diffusion tensor D. Let $C : \mathbf{x} = \mathbf{x}(t'), 0 < t' < t$ be a segment of stochastic trajectory between times zero and $t > 0$. We define the area two-form $A(t)$ associated with this segment with components

$$A_{ij}(t) := \frac{1}{2}\int_C x_i dx_j - x_j dx_i = \frac{1}{2}\int_0^t (x_i \dot{x_j} - x_j \dot{x_i})(t')dt'. \tag{29}$$

This two-form has a simple geometric interpretation. To see this, let $\mathbf{a}$, $\mathbf{b}$ be two linearly independent vectors in $\mathbb{R}^N$. We can map the N-dimensional configuration space into a two-dimensional plane whose coordinates are

$$y_1 = a_i x_i, \quad y_2 = b_i x_i, \tag{30}$$

where the repeated index i implies summation from 1 to N. For example, one can think of y_1 and y_2 as a pair of independent, experimentally measurable observables. Let c be the image of C in the y_1, y_2 plane. Then, the line integral

$$\mathscr{A}(t) := \frac{1}{2}\int_c y_1 dy_2 - y_2 dy_1 \tag{31}$$

represents an oriented area swept out between times zero and t (cf. Fig. 6). Notice that clockwise loops caused by self-intersection give negative contributions to $\mathscr{A}(t)$. It should also be noted that, provided that the Jacobian J of the deterministic flow is a stable node (i.e., all eigenvalues are real and negative), the projected fluctuation loops are expected in general to be topologically equivalent to circles [20]. By contrast, for linear systems with other types of equilibrium points (e.g., spirals) and certainly for nonlinear systems the possibility of nontrivial folds in the projected fluctuation loops cannot be dismissed.

The area tensor defined here is related to the probability angular momentum tensor recently introduced to describe the dynamics of nondetailed balance systems that move in

discrete or continuous spaces [23–25]. An important difference between the two is that while the probability angular momentum tensor explicitly depends on the velocity field, the area tensor does not. Additionally, it should be noted that a general circulation expression has recently been introduced for general N-dimensional stochastic dynamical systems [26]; the area tensor defined here is closely related to the projection of this expression onto an arbitrary two-dimensional plane. Substituting (30) into (31), we derive the relation of $\mathscr{A}(t)$ to $A(t)$,

$$\mathscr{A}(t) := \frac{a_i b_j}{2} \int_C (x_i dx_j - x_j dx_i) = A_{ij}(t) a_i b_j. \tag{32}$$

Next, we analyze the time evolution of the ensemble average $\langle A\rangle(t)$. Evoking the stochastic ODE (2) for $\mathbf{x}(t)$, we have

$$\begin{aligned}\langle A_{ij}\rangle(t) &:= \frac{1}{2}\int_0^t [J_{jk}\langle x_i x_k\rangle(t') - J_{ik}\langle x_j x_k\rangle(t')]dt' \\ &\quad + \frac{1}{2}\int_0^t (\sigma_{jk}\langle x_i w_k\rangle - \sigma_{ik}\langle x_j w_k\rangle)dt'. \end{aligned}\tag{33}$$

In Appendix A, we show that

$$\langle x_i w_k\rangle = \sigma_{ik}, \tag{34}$$

so that the second integral on the right hand side of (33) vanishes. This leaves

$$\begin{aligned}\langle A_{ij}\rangle(t) &= \frac{1}{2}\int_0^t [J_{jk}\langle x_i x_k\rangle(t') - J_{ik}\langle x_j x_k\rangle(t')]dt' \\ &= \frac{1}{2}\int_0^t [m(t')J^T - Jm(t')]_{ij}dt', \end{aligned}\tag{35}$$

where $m_{ij} = \langle x_i x_j\rangle$ are the components of the second moment tensor. The component-free form is

$$\langle A\rangle(t) = \frac{1}{2}\int_0^t [m(t')J^T - Jm(t')]dt'. \tag{36}$$

From the Fokker-Planck equation associated with the stochastic ODE (2), one can show that the second moment tensor satisifies the matrix ODE

$$mJ^T = \dot{m} - Jm - 2D. \tag{37}$$

The calculation behind (37) is reviewed in Appendix A along with a useful extension. The time-independent version of (37) is typically referred to as the fluctuation-dissipation relation for the stochastic process [3]. By (12), the mapping tensor M satisfies the same fluctuation-dissipation relation. Furthermore, if we assume that all the eigenvalues of J have negative real part, then it is straightforward to show that $m(t) \to M$ as $t \to \infty$; this convergence is exponentially fast with time scale determined by the deterministic relaxation time, i.e., the inverse of the (negative) eigenvalue of J with smallest magnitude [3,20]. By (37), we can substitute for mJ^T in (36) to find

$$\begin{aligned}\langle A\rangle(t) &= \int_0^t \left(\frac{1}{2}\frac{dm}{dt'} - Jm(t') - D\right)dt' \\ &= \frac{1}{2}[m(t) - m(0)] - \int_0^t [Jm(t') + D]dt'. \end{aligned}\tag{38}$$

Due to the rapid convergence of $m(t)$ to M, we have for times t large compared to the deterministic relaxation time the following asymptotic relation:

$$\langle A\rangle(t) \sim -(JM + D)t, \tag{39}$$

provided that $JM + D \neq 0$. On the other hand, if $JM + D = 0$, then one can show directly from (37) that $\langle A\rangle(t) \sim 0$ at long times, so that (39) is valid in either case. Taking the time derivative of (39), we have

$$\frac{d\langle A\rangle}{dt} \to -(JM + D) \quad \text{as } t \to \infty. \tag{40}$$

If the stochastic dynamical system (2) has detailed balance, then it is easy to show directly that $JM + D = 0$. We can see this by noting that, for a detailed balance system, the probability current (3) associated with the time-independent probability density vanishes, so that

$$J_{ij}x_j\rho - D_{ij}\partial_j\rho := 0. \tag{41}$$

Multiplying by x_k, and integrating over all space with respect to $\mathbf{x}$, we obtain

$$J_{ij}m_{jk} - D_{ik} = 0, \tag{42}$$

where we are assuming that the eigenvalues of J all have negative real part. In this case, m is really the mapping tensor, and (42) is just the component form of $JM + D = 0$. Conversely, $JM + D \neq 0$ implies the breaking of detailed balance which can be detected by asymptotic linear growth of the area two form as $t \to \infty$. In practice, one picks experimental coordinates y_1 and y_2 made from linear combinations of the "original" coordinates $x_1, \ldots, x_N$, and a linear growth of the area $\mathscr{A}(t)$ in (32) is observed. The asymptotic rate of

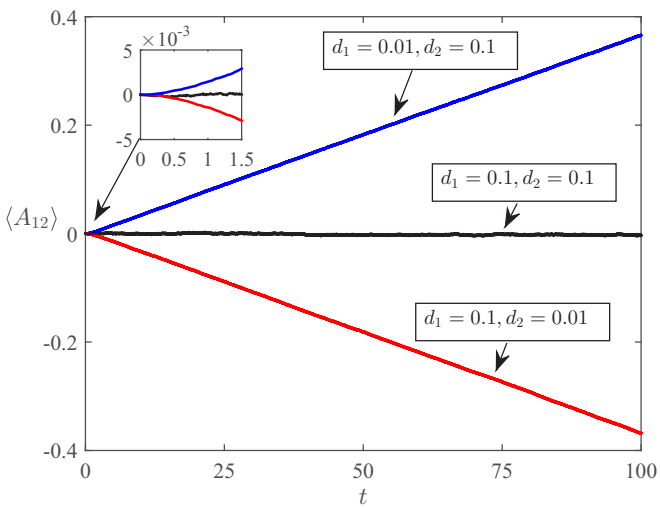

FIG. 7. Numerically determined stochastic area function for three cases: clockwise vorticity ($d_1 = 0.01$, $d_2 = 0.1$), detailed balance ($d_1 = d_2 = 0.1$), and counterclockwise vorticity ($d_1 = 0.1$, $d_2 = 0.01$). The inset shows expected quadratic dependence for short times. These plots are generated using Euler-Maruyama iteration of (17) to determine the area function using (29). The area was then averaged over 1000 trials.

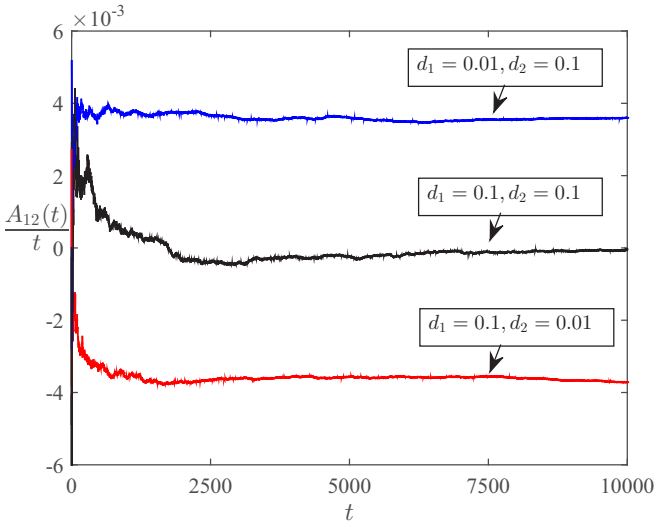

FIG. 8. Here we show the swept area divided by time for one long stochastic trial, i.e., there is no ensemble averaging in this case. Note that this scenario is relatively easy to implement for a real experiment.

growth is

$$\frac{d\langle \mathscr{A} \rangle}{dt} \to -(JM + D)_{ij} a_i b_j. \tag{43}$$

In Fig. 7, the ensemble-averaged area tensor versus time is numerically computed for the two-dimensional circuit system (17). At long times, the linear dependence with time is clear and is fully consistent with the analytical prediction (40). At short times (relative to the deterministic relaxation times, that is), the time dependence for nondetailed balance systems exhibits quadratic behavior which can be analytically confirmed by evaluating (33) in the appropriate limit.

Figure 8 shows the behavior of $A_{12}(t)/t$ for *individual* stochastic trials over much larger time intervals than used in the preceding figure. At shorter times, the behavior is erratic and trial dependent with large differences between different trials. However, we find that for sufficiently long times, the ratio $A_{12}(t)/t$ approaches the ensemble averaged value as in (40), that is,

$$\frac{A_{12}(t)}{t} \to \frac{d\langle A_{12} \rangle}{dt} \to -(JM + D)_{12} \quad \text{as } t \to \infty. \tag{44}$$

This is significant because, in many experimental systems, it is impractical to compute ensemble averages directly from data. On the other hand, one typically does collect individual time series of great length, suggesting the usefulness of Eq. (44) as an potentially useful metric for discerning the presence or lack of detailed balance directly from experimental data.

V. CONCLUSIONS

In this paper, we have solved the effective Hamilton equations of large deviation theory to analytically determine the fluctuational and relaxational trajectories for linear stochastic dynamical systems that generally do not obey detailed balance. In particular, a mapping tensor has been defined that allows the straightforward construction of the most-probable fluctuational trajectory in terms of the momentum solutions to the Hamilton equations. Interestingly, the mapping tensor is closely related to the time-dependent second moment tensor of the system; in fact, if the fixed point is a stable equilibrium, then the mapping tensor is precisely the infinite time limit of the second moment tensor. We have explicitly constructed fluctuation loops for an experimentally realistic circuit model consisting of coupled RC elements, where each element is driven by its own independent noise source.

Another important result of this paper concerns the role of the area tensor as a quantitative indicator of detailed balance breaking in any noise-driven linear dynamical system. The relevance of the area tensor to experimental noisy systems, such as those mentioned in the Introduction, is succinctly summarized as follows: take any two independent variables of linear stochastic dynamics and look at the area $\mathscr{A}(t)$ swept out in the plane of those variables for a single trial. Provided that the time series is sufficiently long, the ratio $\mathscr{A}(t)/t$ approaches a constant value at large t. When this value is nonzero, the stochastic dynamics break detailed balance, and we know this, independent of any detailed knowledge about the system, other than the linearity of the deterministic flow and the constancy of the diffusion tensor.

APPENDIX A: DERIVATION OF THE FLUCTUATION-DISSIPATION RELATION AND A USEFUL EXTENSION THEREOF

Let $\rho(\mathbf{x},t)$ be the ensemble probability density in configuration space. The second moment tensor $m = m(t)$ has components

$$m_{ij} = \langle x_i x_j \rangle := \int x_i x_j \rho(\mathbf{x},t) d\mathbf{x}. \tag{A1}$$

From the Fokker-Planck equation governing $\rho(\mathbf{x},t)$,

$$\rho_t + \nabla \cdot (J\mathbf{x}\rho - D\nabla\rho) = 0, \tag{A2}$$

we derive the evolution equation (12) for $m(t)$. Let $g(\mathbf{x})$ be any test function. Its ensemble average is

$$\langle g \rangle(t) := \int g(\mathbf{x}) \rho(\mathbf{x},t) d\mathbf{x}. \tag{A3}$$

Mutiplying (A2) by $g(\mathbf{x})$, integrating over $\mathbf{x}$, and using the divergence theorem, we find that its time rate of change is

$$\frac{d}{dt}\langle g \rangle = \int \rho[J\mathbf{x} \cdot \nabla g - \nabla \cdot (D\nabla g)] d\mathbf{x}. \tag{A4}$$

Taking $g(\mathbf{x}) = x_i x_j$, Eq. (A4) becomes

$$\begin{aligned} \dot{m}_{ij} &= \int \rho[(J_{kl}x_l)\partial_k(x_i x_j) + \partial_k(D_{kl}\partial_l(x_i x_j))] d\mathbf{x} \\ &= \int \rho(J_{il}x_l x_j + x_i x_l J_{jl} + 2D_{ij}) d\mathbf{x} \\ &= (Jm + mJ^T + 2D)_{ij}, \end{aligned} \tag{A5}$$

which is the component form of (37).

An extension of (37) allows us to show that

$$\langle x_i w_j \rangle = \sigma_{ij}, \tag{A6}$$

which arises in Sec. IV in the analysis of the area tensor. The idea is to introduce the unit Brownian motions

$$B_i(t) := \int_0^t w_i(t')dt' \tag{A7}$$

as additional coordinates in a $2N$-dimensional stochastic dynamics,

$$\dot{\mathbf{x}} = J\mathbf{x} + \sigma\mathbf{w}, \quad \dot{\mathbf{B}} = \mathbf{w}. \tag{A8}$$

Here $\mathbf{B} := (B_1, \ldots, B_N)$ is the vector of Brownian motions, and the $2N \times 2N$ Jacobian, noise and diffusion tensors of this expanded stochastic dynamics take block forms, respectively,

$$\begin{pmatrix} J & 0 \\ 0 & 0 \end{pmatrix}, \quad \begin{pmatrix} \sigma & 0 \\ I & 0 \end{pmatrix}, \quad \begin{pmatrix} D := \sigma\sigma^T & \sigma \\ \sigma^T & I \end{pmatrix}. \tag{A9}$$

Here, I is the $N \times N$ identity tensor. The second moment tensor of the expanded system has block form

$$\begin{pmatrix} m & m' \\ m'^T & 2tI \end{pmatrix}, \tag{A10}$$

where the off-diagonal block m' has components $m'_{ij} = x_i B_j$, and the lower right block comes from $\langle B_i B_j \rangle = 2t\delta_{ij}$. The time-dependent fluctuation-dissipation equation with the expanded Jacobian, diffusion, and second moment tensors in (A9), (A10) reproduces (37) for m and, for the "off diagonal" block m', we have

$$\dot{m'} = Jm' + 2\sigma, \tag{A11}$$

a key expression for evaluating $\langle x_i w_j \rangle$. Time differentiation of $m'_{ij} = x_i B_j$ and use of the stochastic ODE (A8) gives

$$\begin{aligned} \dot{m'}_{ij} &= \langle \dot{x}_i B_j + x_i \dot{B}_j \rangle \\ &= \langle J_{il} x_l B_j + \sigma_{il} w_l B_j + x_i w_j \rangle \\ &= (J\mu' + \sigma)_{ij} + \langle x_j w_j \rangle. \end{aligned} \tag{A12}$$

The last line uses $w_l B_j = B_j \dot{b}_l = \delta_{jl}$. Comparing (A11) and (A12), we see that $\langle x_i w_j \rangle = \sigma_{ij}$ as in (A6).

APPENDIX B: THERMODYNAMIC INTERPRETATION OF STOCHASTIC VORTICITY

In the RC network of Sec. III, we assume that the two resistors are immersed in heat baths of temperatures T_1 and T_2. The thermal fluctuations of the voltage across these resistors are modeled as white noise voltage sources $\delta v_i(t) = s_i w_i(t)$, $i = 1,2$. The noise amplitudes s_i are related to the bath temperatures T_i by [27]

$$s_i = \sqrt{2Rk_B T_i}. \tag{B1}$$

From the circuit differential equation (17), we derive the energy identity:

$$\begin{aligned} &\frac{d}{dt}\left(\frac{1}{2}c\left({v_1}^2 + {v_2}^2\right) + \frac{1}{2}C(v_2 - v_1)^2\right) \\ &\quad = -\frac{{v_1}^2}{R} + \frac{s_1 v_1}{R} w_1(t) - \frac{{v_2}^2}{R} + \frac{s_2 v_2}{R} w_2(t). \end{aligned} \tag{B2}$$

The left hand side is the rate of change of energy stored in the capacitors. In the right hand side, ${v_1}^2/R$ and ${v_2}^2/R$ are rates of heat dissipation into the baths of temperature T_1 and T_2, respectively. Evidently, the remaining terms $s_1 v_1 w_1(t)/R$ and $s_2 v_2 w_2(t)/R$ are the rates of work done by the respective baths through the voltage fluctuations they induce. Hence

$$r_i := -\frac{{v_i}^2}{R} + \frac{s_i}{R} v_i w_i, \quad i = 1,2, \tag{B3}$$

is the net rate of energy transfer into the bath of temperature T_i. We examine the ensemble average energy transfer rates under stationary conditions. Ensemble averages $\langle {v_i}^2 \rangle$, $\langle v_i w_i \rangle$ can be computed from an extension of the fluctuation-dissipation relation. The calculation here exploits a connection between the energy transfer rates and the area tensor of the stochastic voltage dynamics. Multiply the first of the circuit differential equations (15) by v_1 to find

$$(C + c)\frac{d}{dt}\left(\frac{1}{2}{v_1}^2\right) - Cv_1\dot{v}_2 = -\frac{{v_1}^2}{R} + \frac{s_1}{R} v_1 w_1 = r_1. \tag{B4}$$

Assuming the $v_i(t)$ have relaxed to stationary processes, ensemble averaging of (B4) gives

$$\langle r_1 \rangle = -C\langle v_1 \dot{v}_2 \rangle. \tag{B5}$$

Interchanging indices 1 and 2 in (B5) shows that $\langle r_1 \rangle$ is opposite and equal to $\langle r_2 \rangle$. Using

$$0 = \left\langle \frac{d}{dt}(v_1 v_2) \right\rangle = \langle v_1 \dot{v}_2 \rangle + \langle \dot{v}_1 v_2 \rangle, \tag{B6}$$

we can recast (B5) as

$$\langle r_1 \rangle = C\langle \dot{A}_{12} \rangle, \tag{B7}$$

where

$$A_{12} = \frac{1}{2}\int_0^t (v_2 \dot{v}_1 - v_1 \dot{v}_2)(t')dt' \tag{B8}$$

is the 12 component of the area tensor. The actual calculation of $\dot{A}_{12}$ is simplified a bit by transforming coordinates from v_1 and v_2 to $x_1 := (v_2 - v_1)/2$, $x_2 := (v_1 + v_2)/2$ as in (16). We have

$$\dot{A}_{12} = \tfrac{1}{2}(v_2 \dot{v}_1 - v_1 \dot{v}_2) \tag{B9}$$

$$= \tfrac{1}{2}[(x_1 + x_2)(\dot{x}_2 - \dot{x}_1) - (x_2 - x_1)(\dot{x}_1 + \dot{x}_2)] \tag{B10}$$

$$= -(x_2 \dot{x}_1 - x_1 \dot{x}_2). \tag{B11}$$

Under stationary conditions, we have from (43)

$$\langle x_2 \dot{x}_1 - x_1 \dot{x}_2 \rangle = -2(JM + D)_{12}, \tag{B12}$$

which can also be written as

$$\langle \dot{A}_{12} \rangle = 2(JM + D)_{12}. \tag{B13}$$

Since the differential equations are nondimensionalized with the scaling unit of time Rc, we obtain from (B13) the time

rate of change of A_{12} in units of $(Rc)^{-1}$. Using the explicit forms of J, D, and M in (19), (21), and (25), and restoring dimensional time, we have

$$\langle \dot{A}_{12} \rangle = \frac{\mu}{4} \frac{1-\mu}{1+\mu} \frac{1}{Rc} \frac{k_B(T_2 - T_1)}{c}. \tag{B14}$$

Finally, using the definition $\mu = (1 + \frac{2C}{c})^{-1}$ we can write (B7) for the ensemble-averaged energy flow rate into the bath of temperature T_1:

$$\langle r_1 \rangle = \frac{1}{8} \frac{(1-\mu)^2}{1+\mu} \frac{k_B(T_2 - T_1)}{Rc}. \tag{B15}$$

As expected, the averaged energy flow rate $\langle r_1 \rangle$ is zero when μ tends to unity, i.e., when the coupling goes to zero. Additionally, $\langle r_1 \rangle$ is proportional to $T_2 - T_1$ which is consistent with the basic nonequilibrium thermodynamics of the coupled RC network.

[1] J. M. Newby, P. C. Bressloff, and J. P. Keener, Phys. Rev. Lett. **111**, 128101 (2013).

[2] C. Penland and P. Sardeshmukh, J. Climate **8**, 1999 (1995).

[3] J. B. Weiss, Tellus Ser. A-Dyn. Metrol. Oceanogr. **55**, 208 (2003).

[4] P. Williams, Philos. Trans. R. Soc. A **363**, 2931 (2005).

[5] J. B. Weiss, Phys. Rev. E **76**, 061128 (2007).

[6] Y. Bomze, R. Hey, H. T. Grahn, and S. W. Teitsworth, Phys. Rev. Lett. **109**, 026801 (2012).

[7] H. B. Chan, M. I. Dykman, and C. Stambaugh, Phys. Rev. Lett. **100**, 130602 (2008).

[8] H. B. Chan, M. I. Dykman, and C. Stambaugh, Phys. Rev. E **78**, 051109 (2008).

[9] C. Battle, C. P. Broedersz, N. Fakhri, V. F. Geyer, J. Howard, C. F. Schmidt, and F. C. MacKintosh, Science **352**, 604 (2016).

[10] J. Gladrow, N. Fakhri, F. C. MacKintosh, C. F. Schmidt, and C. P. Broedersz, Phys. Rev. Lett. **116**, 248301 (2016).

[11] D. G. Luchinsky and P. V. E. McClintock, Nature (London) **389**, 463 (1997).

[12] D. G. Luchinsky, P. V. E. McClintock, and M. I. Dykman, Rep. Prog. Phys. **61**, 889 (1998).

[13] P. H. Dannenberg, J. C. Neu, and S. W. Teitsworth, Phys. Rev. Lett. **113**, 020601 (2014).

[14] D^{-1} and J have physical units L^2T^{-1} and T^{-1}, respectively, so $D^{-1}J$ has units L^{-2} .

[15] M. I. Freidlin and A. D. Wentzell, *Random Perturbations of Dynamical Systems*, A Series of Comprehensive Studies in Mathematics (Springer, New York, 2012).

[16] M. Heymann and E. Vanden-Eijnden, Commun. Pure Appl. Math. **61**, 1052 (2008).

[17] R. S. Maier and D. L. Stein, SIAM J. Appl. Math. **57**, 752 (1997).

[18] H. Xu and S. W. Teitsworth, J. Appl. Phys. **108**, 043705 (2010).

[19] D. G. Luchinsky, R. S. Maier, R. Mannella, P. V. E. McClintock, and D. L. Stein, Phys. Rev. Lett. **82**, 1806 (1999).

[20] J. C. Neu, A. Ghanta, and S. W. Teitsworth (unpublished).

[21] S. Barnett, *Introduction to Mathematical Control Theory* (Oxford University Press, Oxford, 1975).

[22] Regarding relation of noise terms to physical units, let T, V stand for time and voltage units. Recall that unit white noise has units $\frac{1}{\sqrt{T}}$ [27]. Hence the noise amplitudes in Fig. 1 have units $\sqrt{T}V$.

[23] R. K. P. Zia and B. Schmittmann, J. Stat. Mech.: Theory Exp. (2007) P07012.

[24] M. S. Shkarayev and R. K. P. Zia, Phys. Rev. E **90**, 032107 (2014).

[25] A. Mellor, M. Mobilia, and R. K. P. Zia, Europhys. Lett. **113**, 48001 (2016).

[26] D. Pinna, A. D. Kent, and D. L. Stein, Phys. Rev. E **93**, 012114 (2016).

[27] C. Gardiner, *Stochastic Methods: A Handbook for the Natural and Social Sciences*, Springer Series in Synergetics (Springer, New York, 2009).